13th Australia New Zealand Conference on Geomechanics – Acosta-Martínez & Lehane (Eds.)

Predicting in-ground buckling instability of the steel H-beam pile through nonlinear analysis

C. Lee & C. Ng
SMEC, Sydney, Australia

R. Kelly
SMEC, Brisbane, Australia

ABSTRACT: In many solar farms, the solar panel array is supported by steel H-beam piles. The ability to design an optimum steel section is dependent on the successful estimation of lateral torsional buckling and global buckling instability under lateral and axial loads. This buckling instability causes the formation of a localised plastic hinge in the pile resulting in a reduction in the structural capacity. The design of steelwork is covered by the Australian Standard AS 4100 (1998), which addresses the buckling instabilities separately, that is the lateral torsional buckling for a beam and axial buckling for a column. The design requires estimation of the effective length based on the end restraint conditions and the equivalent unsupported length of steel H-beam pile. Owing to the ground-structure interaction between the pile and the foundation, the estimation of the effective length of the steel H-beam pile based on the pile restraint conditions is not well-defined. Often a conservative assumption that the effective length is the length to the point of fixity below ground i.e. the point of zero deflection under a buckling analysis is adopted for the steel H-beam design. This paper presents the use of 3D plate element nonlinear finite element analysis in MIDAS Civil 2018 for the steel H-beam design embedded in clay. Parametric studies to simultaneously consider the effects of the nonlinear soil-structure interaction, the P-delta effect generated by the axial load and the nonlinearity of the steel material was undertaken. The results from the analysis are compared with the simplified approach based on the point of fixity below ground. The results show that the unsupported length is not only dependent on the ground strength, but also the relative stiffness between the steel section and the stiffness of the ground, which must be considered in order to achieve a safe and economical design.

1 INTRODUCTION

1.1 *Solar panel foundation*

In many large-scale solar farms, the solar panel array is supported by an array of small steel H-beam piles partially driven into the ground. A section of unsupported steel H-beam is left as a cantilever above the ground to serve as a mounting column for the horizontal beam that houses the solar panel array, as shown in Figure 1.

These piles are subjected to a relatively high lateral load from the wind and compression load from the self-weight of solar panels. A slender steel H-beam section is typically used, and the steel section may buckle if they are installed through a ground layer with relatively low lateral resistance such as firm clay above a competent stiff stratum. The critical buckling load often became the limit of capacity for such piles.

As such, the ability to achieve an optimum H-beam pile design is therefore dependent on the successful assessment of lateral torsional buckling and global buckling instability.

1.2 *Buckling of piles*

Buckling of slender structural elements is a common concern among the structural engineers. However, the behaviour of the steel H-beam pile is different than a standard column, owing to part of the pile is embedded in the soil that provides lateral support. As such, there is significant soil-structure interaction involved.

Several researchers have addressed the buckling of piles during driving under high compression loads and zero lateral loads. Their results generally support the conclusion that buckling is likely to occur in soils with poor strength properties (Bjerrum 1957; Davisson 1963) or liquefiable soil (Bhattacharya & Bolton 2004) or in soft stratum (Granholm 1929) where the pile could well be designed as a free-standing column. Effects of high lateral loading on the buckling of slender steel H-beam pile were generally limited.

This paper discusses the buckling instability in the context of laterally loaded slender steel H-beam pile and some of the challenges associated with the commonly adopted buckling design for steel H-beam pile

and then presents the results from the 3D finite element analysis (FEA) that simultaneously considered geometric and material nonlinearity.

2 BUCKLING BEHAVIOUR

2.1 *Euler's critical compression load*

The behaviour of a pile can be described as a column carrying loads and the flexure behaviour is closely related to the Euler buckling loads (Timoshenko & Gere 1961). The formulation of the pile flexure subject to an axial force is given as (Heelis et al. 2004):

$$EI\frac{d^4y}{dx^4} + \left[P_0 - \int_0^x f(x)\right]\frac{d^2y}{dx^2} - f(x)\frac{dy}{dx} + k(x)y = 0 \qquad (1)$$

where EI is the flexural rigidity of the pile, P_0 is the external axial compressive force applied at the top of the pile at $x = 0$, $f(x)$ is the friction per unit length, $k(x)$ is the modulus of subgrade reaction and y is the deformation.

Equation 1 implies that if part of the soil surrounding the pile has low friction or the pile is free-standing, this would then lead to $f(x) = 0$ and $k(x) = 0$ and the solution to the differential equation for the force P_0 reduces to Euler's buckling equation, as given in equation 2.

$$P_{cr} = \frac{\pi^2 EI}{(k_e l)^2} \qquad (2)$$

where k_e is the pile effective length factor and l is the unsupported length. The parameter k_e is a non-dimensional multiplier with a theoretical range of 0.5 to 2.0 depending on the rotation and translation fixity/end restraint conditions.

2.2 *Effect of lateral load in buckling*

For a partially embedded pile that is subjected to both vertical and lateral loads, the lateral deformation exacerbates the instability of the pile. Rankine (1866) recognised that the failure load predicted by Equation 2 is more than the actual failure load. This is due to the Euler's critical compression load is sensitive to lateral deformation of the pile.

The lateral loads lead to the generation of bending moment and the lateral deformation or imperfections in the verticality will also result in the generation of a second-order moment from the axial force, P_0 due to the P_0-delta effect, as illustrated in Figure 2a. The lateral deflection changes the cross-section stress state from small eccentric compression to large eccentric compression. A tensile region appears, and this, in turn, reduces the effective compression area and results in an increase in maximum compression stress. There are two possible scenarios in which the steel H-beam could fail, viz: (A) tensile failure when the maximum tensile stress exceeds the steel yield stress or (B) the compression failure when the maximum compression stress exceeds the steel yield stress. In addition, as the axial compression load approaches Euler's critical compression load, the lateral deflection is amplified (Bhattacharya et al. 2005) and additional deflection accelerates the failure.

Figure 1. Solar farms with panel array supported on Steel H-beam pile (photograph courtesy of NEXtracker).

3 AUSTRALIA STANDARD STEELWORK DESIGN

3.1 *Piles subject to axial compression*

The design of steel H-beam pile is covered by Australian Standard AS 4100 (1998) *Steel Structures*. AS 4100 (1998) stipulated that the design of axial compression shall satisfy both the section capacity i.e. the design axial load < yield stress of steel, and member capacity, which accounts for flexural buckling limit of the steel. The flexural buckling limit is dependent on the slenderness of the H-beam pile and is a function of the effective length ($l_e = k_e l$).

Figure 2 shows a free-head pile with an unsupported length L_u and an embedded length L. The lateral load V, moment M, and axial load P_0 cause the pile to deflect with respect to the coordinate axes as shown. Figure 2b shows a free-standing pile with an equivalent unsupported length l which is equal to L_u plus the depth to the point of fixity L_x. This equivalent length of free-standing pile is presumed to behave in the same manner as the system in Figure 2a.

From the structural design viewpoint, the most desirable simplification is to consider the lower end of

the pile as fixed at some depth below the ground surface, which results in member effective length factor $k_e = 2$. The corresponding theoretical *effective* unsupported length is then equal to $l_e = k_e l = 2l$.

Furthermore, if the pile head in Figure 2b is attached to a beam, the design would complete more efficiently if the loads V, M, and P_0 acting on each pile head could be determined. This can be accomplished with a structural frame analysis in which the bending of the pile becomes a function of the buckling load of the pile.

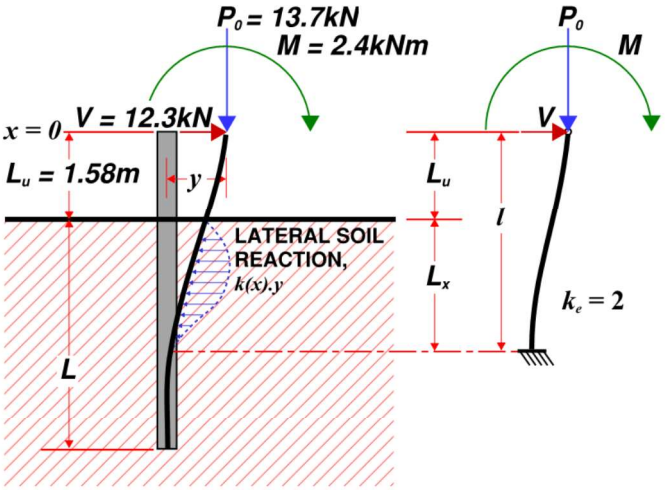

Figure 2a Figure 2b

Figure 2. Soil-pile interaction (Figure 2a). The idealisation of global buckling design to AS 4100 (1998) (Figure 2b).

3.2 *Piles subject to bending*

For steel H-beam subjected to bending without full lateral restraint, AS 4100 (1998) stipulated that steel member shall be designed so that the applied moment is less than the member moment capacity. The member moment capacity (M_b) is dependent on the section geometry, slenderness and buckling moment limit of the steel H-beam. The buckling moment limit is again a function of the effective length:

$$l_e = k_t k_l k_r l \quad (3)$$

where k_t, k_l and k_r is the twist restraint factor, load height factor and lateral rotation restraint factor, and l is the equivalent unsupported length in Figure 2b.

3.3 *Piles subject to axial and bending*

Once the axial and bending effects are evaluated, the combined actions shall be proportioned so that the pile bending stress (M^*) is within both the section and member capacity. The simplified expression is given as follows:

$$M^* \leq \text{Min}[\, M_s(1 - P_0/N_s), M_b(1 - P_0/N_c)\,] \quad (4)$$

where M_s and N_s are the section moment and axial load capacity determined from the yield stress of steel and effective section modulus, M_b and N_c are the member moment and axial load capacity considering the buckling effect.

As seen, the main difficulty of the structural design is the determination of the depth L_x (or l) for both effects of axial load buckling and lateral torsional buckling, which either must be assumed arbitrarily or conservatively taken as the depth to fixity with zero deflection i.e. the point of zero deflection under a buckling analysis, according to some method of analysing the embedded portion of the pile. Neither of these procedures fully addresses the complexity of the problem. Moreover, it is also unclear how realistic or conservative the design developed based on depth to fixity with zero deflection.

4 FINITE ELEMENT ANALYSIS (FEA)

4.1 *Pile equivalent unsupported length*

Parametric studies on buckling of piles was undertaken using MIDAS Civil 2018 to assess the equivalent unsupported length of steel H-beam (l) embedded in a clay layer with different consistencies. MIDAS is a 3D structural finite element software that is capable of simultaneously considering the soil nonlinear responses and the effects of the material and geometric nonlinearity. The equivalent unsupported length back-calculated from FEA for different steel H-beam embedded in clay with various consistencies was then compared with the depth to the point of fixity in the ground.

4.2 *Steel H-beam pile*

Table 1 presents some of the most commonly used steel H-beam sections to support the solar panel array and the relevant properties modelled in the FE parametric studies.

Table 1. Steel H-beam pile

Type	d	b_f	t_f	t_w	A_g	I_x
	m	m	mm	mm	$\times 10^{-3}$m^2	$\times 10^{-6}$m^4
W6×16	0.16	0.1	10.3	6.6	3.02	13.4
W6×12	0.15	0.1	7.1	5.8	2.26	9.20
W6×9	0.15	0.1	5.5	4.3	1.69	6.24

Note:
1. d – Depth of section, b_f – Width of flange, t_f – Thickness of flange, t_w – Thickness of web, A_g – Gross area of cross section, I_x – Second moment of inertia about x–axis
2. Modulus of elasticity = 2×10^8kN/m^2. Density = 78.5kN/m^3. Yield stress = 350MPa.

4.3 *Subsurface model*

Table 2 presents the consistency of the ground included in the parametric studies. MIDAS Civil 2018 model the soil using the Winkler method or the subgrade reaction method. The method was first introduced by Winkler (1867) to analyse the response of

beams on an elastic subgrade by characterising the soil as a series of independent linearly-elastic soil springs. The soil spring defines the soil resistance (kN) for a unit deflection (m), as shown in Figure 3. The spring stiffness can be derived from the subgrade reaction modulus (lateral pressure resistance over deformation) and the limiting lateral soil capacity (p_y).

A reasonable method for evaluating the subgrade reaction modulus (e.g. Poulos 2012) is using Vesic (1961):

$$k(x)D = K = 0.65\sqrt[12]{\frac{E_s D^4}{EI}}\left(\frac{E_s}{1-\nu^2}\right) \quad (5)$$

where D = pile diameter, E_s and ν is the ground elasticity and Poisson's ratio, and EI is the flexural rigidity of the pile. Bowles (1997) recommends using double the Vesic (1961) value for the laterally loaded pile case on the basis that Vesic (1961) assumes a strip footing at ground surface whereas soil surrounds a pile producing a considerable side shear resistance. This is in line with what was proposed by Carter (1984) and Ling (1988), who found that the closest agreement in predicting the pile deflection was obtained by using a factor of 1 (instead of 0.65) in Equation 4. As such, Table 2 assumes K linearly increases from the surface to a value of 2 times at a depth of $3D$.

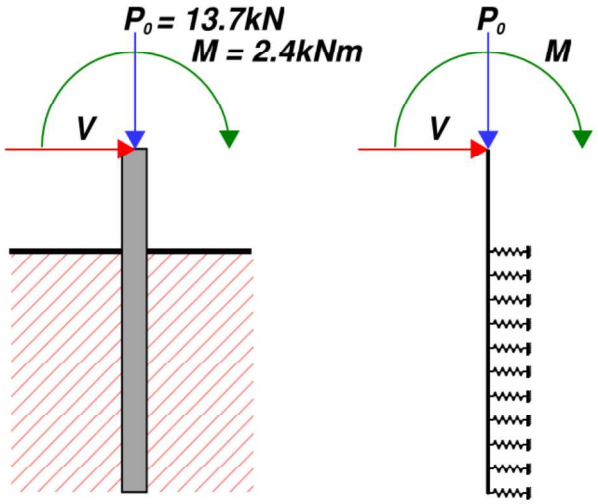

Figure 3a Figure 3b

Figure 3. Implementation of Winkler Spring Concept for the laterally loaded pile. Pile subjected to lateral load (Figure 3a). Idealised using Winkler spring method in FEA (Figure 3b).

Table 2. Ground parameters.

Ground Consistency	S_u kPa	ν -	E_s MPa	P_y Note 1 kPa	$K=k(x)D$ Note 2 MPa
Very Soft	6	0.3	1.5	$2S_u$ to $9S_u$	0.5 to 1
Soft	12	0.3	3	$2S_u$ to $9S_u$	1 to 2
Firm	25	0.3	6	$2S_u$ to $9S_u$	2 to 4
Stiff	50	0.3	15	$2S_u$ to $9S_u$	6 to 12

For cohesive soils, the limiting lateral soil pressure p_y may be taken to be a linear increase in $2S_u$ at the surface to a value of $9S_u$ at a depth of $3D$, where D is the pile diameter.

In the FEA, a linearly elastic-perfectly plastic spring stiffness was used by defining the soil resistance (kN) for a unit deflection (m). The plastic force (F_p) and the deformation at the point of yielding (δ_p) are calculated as follows:

$$F_p = p_y D L_i \quad (6)$$

$$\delta_p = \frac{F_p}{k(x)DL_i} = \frac{p_y}{k(x)} \quad (7)$$

where L_i is the vertical interval of the spring.

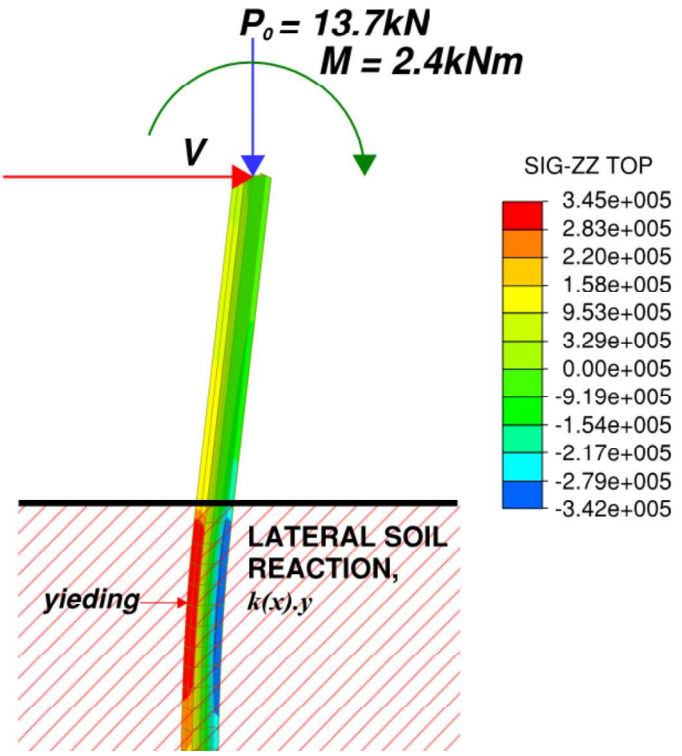

Figure 4. Yielding of the steel H-beam pile during nonlinear FEA.

4.4 *MIDAS Nonlinear analysis*

In the FEA, the H-beam's flange and web were modelled as an individual plate element with von Mises yield criterion, which is based on the plasticity theory that applies best to ductile materials such as metals and with the dimension shown in Table 1.

The typical pile loads are summarised in Figure 2a. The P_0 and V are predominately due to the self-weight of the solar panel and wind load. In the FEA, The P_0 and M were kept constant, while the V was incrementally increased until the steel H-beam pile reaches its ultimate yield stress. Figure 4 shows the typical output from the analysis and the result showing that the flange of the H-beam was reached the yield strength of the steel. The steel H-beam's member moment capacity (M^*) is then equal to the maximum bending moment calculated right before the yield of steel. The M^* was used to back-calculated the equivalent unsupported length (l) using the analytical method. The l

was then compared with the free-standing length (L_u) and depth to the depth to the point of fixity ($L_u + L_x$) in the ground with zero deflection.

5 RESULTS AND DISCUSSION

5.1 *Moment capacity*

Table 3 presents the moment capacity assessed using the standard steelwork design and that assessed using the nonlinear FEA method. For the standard steelwork design, the depth to the point of fixity reported in Table 5 was used. The aim is to compare the calculated moment capacity using the standard steelwork design (Figure 2b) to that predicted by the nonlinear FEA method. For the common steel sections used to support the solar panel array, the results indicate that the moment capacity determined from the conventional approach is about 59% to 94% of that assessed from the FEA (Table 4). Values in brackets are from the nonlinear FEA method

Table 3. Comparison of moment capacity (kNm) using standard steelwork design and nonlinear FEA method

Consistency	W6×16	W6×12	W6×9
Soft	34 (36)	22 (29)	14 (21)
Firm	35 (42)	23 (33)	15 (24)
Stiff	38 (47)	25 (35)	16 (27)

Table 4. Ratio of moment capacity using standard steelwork design to nonlinear FEA method

Consistency	W6×16	W6×12	W6×9
Soft	0.94	0.76	0.67
Firm	0.83	0.70	0.63
Stiff	0.81	0.71	0.59

5.2 *Equivalent unsupported length*

Table 5 presents a comparison of the depth to the point of fixity ($L_u + L_x$) with zero pile deflection and corresponding equivalent unsupported length (l) from the FEA. For the common steel sections used to support the solar panel array, the results indicate that the equivalent unsupported length is about 58% to 91% of the depth to the point of fixity (Table 6). As such, when the depth to fixity corresponding to the zero deflection under buckling analysis below ground is used to assess the structural capacity of small steel H-beam piles partially driven into the ground, it will lead to under prediction in the steel member capacity under lateral torsional buckling effect and resulted in a conservative steel section design.

The results also show that a stronger steel section, in general, has a much longer equivalent unsupported length than the weaker counterpart. For instance, the equivalent unsupported length for the W6×16 installed in soft clay is 2.82m, compared to 1.68m for the W6×9. One plausible explanation for this observation is that the ground is more proficient at reducing the unsupported length for a weaker steel section than a stronger steel section. For a weaker steel section installed in a firm or better ground, the equivalent unsupported length is essentially equal to the free-standing height left cantilever above the ground ($l = L_u$ = 1.58m). For a stronger section (W6×16), the ground will need to provide a greater support in order to reduce the equivalent unsupported length to the free-standing height.

Table 5. Depth to point of fixity and equivalent unsupported length

Consistency	W6×16	W6×12	W6×9
Soft	3.09 (2.82)	2.99 (1.95)	2.89 (1.68)
Firm	2.84 (2.08)	2.76 (1.58)	2.68 (1.58)
Stiff	2.58 (1.73)	2.51 (1.58)	2.45 (1.58)

Note:
1. Value in brackets = nonlinear FEA

Table 6. Ratio of equivalent unsupported length to the point of fixity

Consistency	W6×16	W6×12	W6×9
Soft	0.91	0.65	0.58
Firm	0.73	0.57	0.59
Stiff	0.67	0.63	0.64

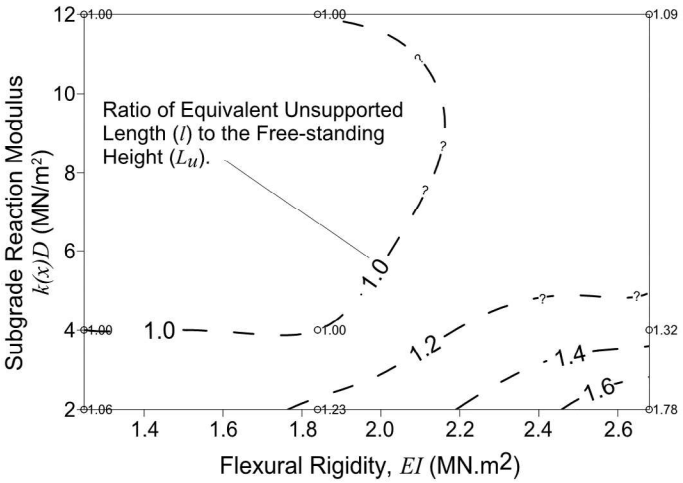

Figure 5. The ratio of equivalent unsupported length to the free-standing height of the H-beam pile.

5.3 *Ground-structure interaction nomogram*

The FEA show that the relative stiffness between the steel section and the stiffness of the ground must be considered in order to achieve a safe and economical design.

Thus, it is desirable to be able to determine the relative stiffness at which the equivalent unsupported length is no longer equal to the free-standing height of the H-beam pile. While the best approach is to undertake a nonlinear FEA outlined in this paper, Figure 5 presents a simplified nomogram developed based on the parametric studies. The nomogram considers the interaction between the stiffness of the ground $k(x)D$ and the flexural rigidity (EI) of the steel H-beam on the equivalent unsupported length (l) and

may be used as a quick guide to determine the equivalent unsupported length of the steel H-beam pile.

6 CONCLUSION

This paper presents the use of 3D plate element nonlinear finite element analysis in MIDAS Civil 2018 for the steel H-beam design embedded in clay. The results show that the equivalent unsupported length for structural design is generally shorter than the depth of fixity and if the depth to fixity is used to assess the structural capacity, it may lead underprediction in the buckling capacity particularly for a smaller steel section. The FEA shows that a stronger steel section, in general, has a much longer equivalent unsupported length than the weaker counterpart. This is because the ground is generally more proficient at reducing the unsupported length for a weaker steel section. The FEA also shows that the unsupported length is not only dependent on the ground strength, but also the relative stiffness between the steel section and the stiffness of the ground. A nomogram was developed based on the parametric studies, which considers the interaction between the stiffness of the ground $k(x)D$ and the flexural rigidity (EI) of the steel H-beam on the equivalent unsupported length (l). The nomogram may be used as a quick guide to assess the equivalent unsupported length of the steel H-beam pile.

REFERENCES

AS4100 1998. Steel structures, *Standard Australia, SAI Global Limited.*

Bhattacharya, S. & Bolton M. 2004. Buckling of piles during earthquake liquefaction, *13th World Conference on Earthquake Engineering*, Vancouver, B.C., Canada, August 2004.

Bhattacharya, S., Carrington, T.M. & Aldridge T.R. 2005. Buckling considerations in pile design, *Frontiers in Offshore Geotechnics: ISFOG* 2005, Gourvenec & Cassidy (eds.), pp. 815–821.

Bjerrum, L. 1957. Norwegian experiences with steel piles to rock, *Geotechnique*, 7(2), pp. 73–96

Bowles, J.E. 1997. Foundation Analysis and Design 5th edition, *The McGraw-Hill Companies, Inc.*, 935 pp.

Carter, D. P. 1984. A non-linear soil model for predicting lateral pile response. *Report No. 359*, Civil Engineering Department, University of Auckland, New Zealand.

Davisson, M.T. 1963. Estimating Buckling Loads for Piles, *Proceedings, 2nd Pan-American Conference on Soil Mechanics and Foundation Engineering, Brazil*, Vol. 1.

Granholm, H. 1929. On the elastic stability of piles surrounded by a supporting medium. *Ingenïors-vetenskaps-Akademiens Handlingar,* No. 89, Stockholm, 56 pp.

Heelis, M.E., Pavlovic, M.N. and West, R.P. 2004. The analytical prediction of the buckling loads of fully and partially embedded piles, *Geotechnique* 54(6), pp. 363–373.

Ling, L. F. 1988. Back analysis of lateral load tests on piles. *Report No. 460*, Civil Engineering Department, University of Auckland.

Poulos, H.G. 2012. Rational assessment of modulus of subgrade reaction, *Geotechnical Engineering Journal of the SEAGS & AGSSEA*, 43(4) December 2012.

Rankine, W.J.M. 1866. Buckling of piles with initial curvature, *Proc of the International Conference on soil mechanics and foundation engineering*, 8, pp. 851–855.

Timoshenko, S. P. & Gere J. M. 1961. Theory of Elastic Stability, *McGraw-Hill Book Company Inc.*

Vesic, A.B. 1961. Beams on elastic subgrade and Winkler's Hypothesis, *Proceeding of 5th ICSMFE*, pp. 845–850.

Winkler, E. 1867. Die lehre von elasticzitat and festigkeit (on elasticity and fixity). *Prague*, pp. 182.